Geophysical Research Letters

RESEARCH LETTER
10.1029/2020GL088100

Sea Ice Retreat Contributes to Projected Increases in Extreme Arctic Ocean Surface Waves

Mercè Casas-Prat[1] **and Xiaolan L. Wang**[1]

[1]Climate Research Division, Science and Technology Directorate, Environment and Climate Change Canada, Toronto, Ontario, Canada

Key Points:

- Changes in surface wind speed alone cannot explain the projected changes in the regional maximum significant wave heights in the Arctic
- The inclusion of a wind predictor that accounts for fetch-limited conditions illustrates that sea ice retreat contributes to wave height increase by increasing fetch
- Sea ice retreat also plays an important role in the projected increases in the regional maximum winds over widening ice-free areas, which in turns affects the regional maximum wave heights

Supporting Information:

- Supporting Information S1

Correspondence to:
M. Casas-Prat,
merce.casasprat@canada.ca

Citation:
Casas-Prat, M., & Wang, X. (2020). Sea ice retreat contributes to projected increases in extreme Arctic ocean surface waves. *Geophysical Research Letters*, *47*, e2020GL088100. https://doi.org/10.1029/2020GL088100

Received 23 MAR 2020
Accepted 30 APR 2020
Accepted article online 10 MAY 2020

Abstract The projected changes and trends in the regional annual and monthly maxima of the significant wave height (H_s) in the Arctic Ocean are studied using wave simulations derived from the CMIP5 (Coupled Model Intercomparison Project Phase 5) climate simulations for 1979–2005 and 2081–2100 periods. Under the RCP8.5 scenario, the regional annual maximal H_s increases on average up to ~3 cm/year, or >0.5%/year, relative to the 1986–2005 climatological value, in many Arctic areas (and up to 0.8%/year in the east side of the Arctic Ocean). While strong winds need to occur for large waves to develop, the changes in wind speed alone cannot explain the increases in the regional maximal H_s. Sea ice retreat also plays an important role by increasing fetch to promote wave growth, thereby contributing notably to the projected increase in wave height. It also contributes to increasing the probability of strong winds over the widening ice-free waters.

Plain Language Summary Significant wave height (H_s) is the average of the highest third of wave heights. Using simulations of historical and future wave climates, we reveal that, under the RCP8.5 scenario, regional annual maximal H_s in the Arctic Ocean and surrounding seas is projected to increase at a rate of up to ~3 cm/year, or equivalently up to 80%, relative to the 1986–2005 climate period, over a 100-year period. While strong winds need to occur for large waves to develop, changes in wind speed alone cannot explain the increases in wave height. Sea ice retreat also plays an important role by increasing the water distance over which wind can blow, thereby promoting wave growth and thus contributing to the increase in wave height. There is also an increase in the probability of strong winds over the widening ice-free waters due to sea ice retreat.

1. Introduction

Recent studies have detected statistically significant positive trends for ocean surface wave heights in the Arctic region over the last decades (e.g., Liu et al., 2016; Semedo et al., 2015; Stopa et al., 2016; Thomson et al., 2016; Wang et al., 2015; Waseda et al., 2018). Wang et al. (2015) found that the increase in the Beaufort-Chukchi-Bering Seas waves cannot be explained by wind speeds alone. Similarly, Thomson et al. (2016) attributed the increase in the mean wave height in the Chukchi and Beaufort Seas to the increasing extent of ice-free waters. Larger open water areas favor the development of long swell waves and higher wind-sea states, as waves are less limited by fetch (Thomson & Rogers, 2014; Thomson et al., 2016). Nevertheless, Waseda et al. (2018) found that the increase of fetch is not a relevant factor in explaining the increase of the largest waves in the Arctic seas, which seem to be strongly correlated by the maximum wind speed in the ice-free water area. Liu et al. (2016) also found a strong correlation between the increase in the extreme wind and the increase in the extreme wave height in the Arctic seas. It is however difficult to isolate the influence of the wind speed alone due to the existing feedback mechanisms between wind and sea ice. Arctic storms are subject to increase in intensity and frequency as a result of sea ice retreat and rising temperatures (Mioduszewski et al., 2018; Rinke et al., 2017; Zhang et al., 2004). In addition, larger ice-free areas increase the chance of the largest winds to occur over water areas where waves can be generated (Liu et al., 2016).

An increase in extreme wave heights is of operational importance to shipping and seabed drilling operations (Thomson et al., 2016). Arctic marine infrastructure might increase throughout this century with the rise of Arctic marine operations due to natural resource development and trade interests (AMSA, 2009). For example, the reduction of the sea ice extent and thickness could enable new routes via the North Pole and/or more traffic of general cargo type vessels (rather than ice-breaking ships) (Aksenov et al., 2017). Understanding the future extreme marine wave conditions is vital to assess future risks, such as oil spills.

Future climate projections show that a September sea ice-free Arctic will most likely be realized between 2045 and 2070 (Laliberté et al., 2016) and therefore the observed trends in wave extremes will likely persist, if not increase at a higher rate. In order to successfully adapt to the climate change challenges and opportunities in the Arctic, it is key to project the future increases in the largest wave heights and to understand the contribution of the main climate drivers. Khon et al. (2014) provided a first useful evaluation of the combined effect of changing surface winds and sea ice retreat on the Arctic wave climate. They found that extreme significant wave heights will increase over different inner Arctic areas due to reduction of sea ice cover and regional wind intensification in the 21st century. However, wave projections therein were poorly sampled (only one climate model was considered), leading to overlooking a large proportion of the wave climate variability (Morim et al., 2019).

This study gains insight into the understanding of the projected future increases in the extreme wave heights in the Arctic seas using recently developed regional wave projections (Casas-Prat & Wang, 2020). In particular, we address the projected increases in the future regional annual/monthly maximal significant wave height (computed over the areas shown in Figure 1) and investigate the roles of wind speed and fetch in these changes. This regional analysis is of interest to moving vessels, as it provides information related to the encountering of large wave heights regardless of their specific location.

2. Data and Methods

The wave projections of Casas-Prat and Wang (2020) span the periods 1979–2005 (historical period) and 2081–2100 (future period) and were obtained using the WAVEWATCH (WW3) wave model (The WAVEWATCH III Development Group (WW3DG), 2016) with a Spherical Multi-Cell (SMC) computational grid (Li, 2012, 2016) of 25-km resolution offshore. The conventional parametrizations of wave physics in WW3 (ST4, NL1 switches) were used (Ardhuin et al., 2010; Hasselmann & Hasselman, 1985), with the Naval Research Laboratory Digital Bathymetry 92 Data Base 2-min resolution (NRL DBDB2). Simulations of hourly significant wave heights (H_s) were obtained by driving WW3 with 3-hourly 10-m surface winds (U10) and daily sea ice concentrations (SICs) produced by five CMIP5 (Taylor et al., 2012) models for the historical and RCP8.5 scenario future period, respectively. The model selection (BCC-CSM1-1, INMCM4, MIROC5, GFDL-ESM2M, and EC-EARTH) aimed to choose models that cover as wide range of uncertainty as possible and to facilitate the Coordinated Ocean Wave Climate Project (COWCLIP) model intercomparison (Hemer et al., 2014; Wang et al., 2015). The resulting simulated extreme wave climatology was compared to the state-of-the-art wave hindcast/reanalysis available for the Arctic region: (i) the latest wave hindcast by the National Centre for Environmental Prediction (NCEP) (https://polar.ncep.noaa.gov/waves/hindcasts/nopp-phase2.php, last accessed June 2018), which was forced by corrected surface winds from the NCEP Climate Forecast System Reanalysis (CFSR) (Saha et al., 2010), and (ii) the latest European Centre for Medium-Range Weather Forecasts (ECMWF) wave reanalysis ERA5 (Copernicus Climate Change Service (C3S), 2017). Note that no waves were generated for SIC > 75% due to sea ice impediment and partial sea ice blocking was imposed for 25% < SIC < 75% (Tolman, 2003). To simplify, in this study, we denote "wave areas" as all areas with nonzero wave energy, including the marginal ice zone (SIC < 75%).

The implemented SIC approach in WW3 is undoubtedly a simplification of the complex ice-wave interactions; different formulations can lead to a considerable source of uncertainty (Thomson et al., 2018). Waves can penetrate into ice-covered seas (Alberello et al., 2019; Kohout et al., 2014) while being attenuated, as a function of the wave period, sea ice concentration, thickness, and floe size distribution (Meylan et al., 2014; Rogers et al., 2016). Moreover, the wave frequency, the ice floe distribution, and the ratio of wave length to ice floe length will determine the ratio of wave scattering (Kohout & Meylan, 2008). Feedback processes such as storm wave-induced ice breakup can also play an important role (Kohout et al., 2014). This is an area of active research under continuous development (Squire, 2020). When more information about the sea ice state is available, typically at shorter time and/or spatial scales, more complex ice-wave interaction approaches might be implemented (e.g., Boutin et al., 2020; Doble & Bidlot, 2013; Liu et al., 2020). However, given the limited knowledge and large uncertainty of the sea ice climatology in the future projections (Shu et al., 2015), the implemented SIC approach in this study is reasonable and similar to those used in wave simulations at similar spatial and temporal scales (e.g., wave projections by Khon et al., 2014, and CFSR and ERA5 historical products). In addition, larger errors are expected to occur in areas with larger SIC. As this study focuses on the annual/monthly regional maximum wave height statistics, which are not expected to occur in the areas of largest SIC, the results thus obtained are less affected by the uncertainty.

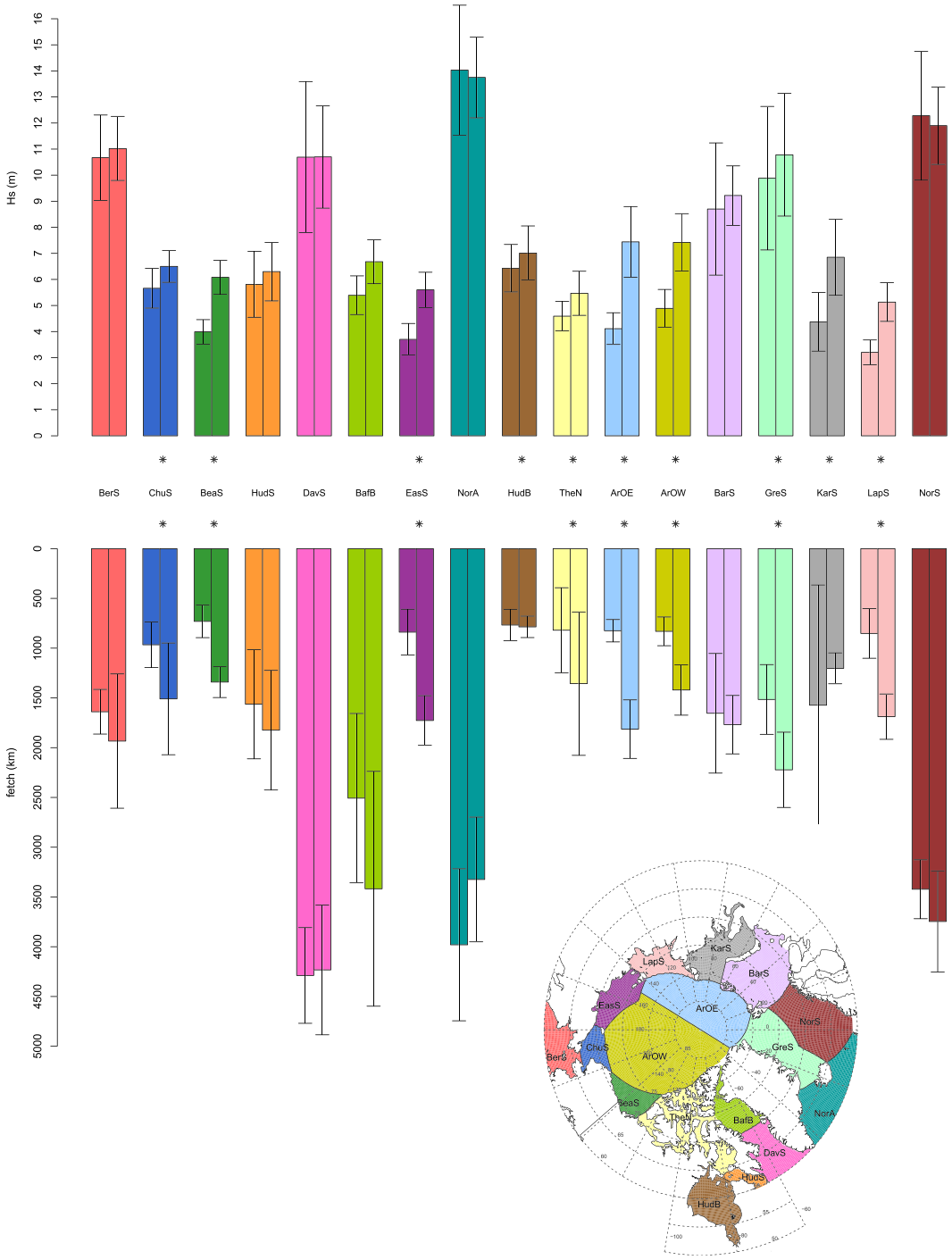

Figure 1. The ensemble average for the historical (left bars) and future (right bars) of (a) $\{H_s\}^{\mathrm{AN}}_{\mathrm{max}}$ and (b) the fetch associated with $\{U10^{w2}_{\mathrm{fetch}}\}^{\mathrm{AN}}_{\mathrm{max}}$, and their 95% confidence intervals. The 17 regions are shown in the map. Asterisks denote the areas with statistically significant projected changes at the 5% level.

The regional annual/monthly regional maxima of H_s, noted as $\{H_s\}^{\mathrm{MON}}_{\mathrm{max}}$ and $\{H_s\}^{\mathrm{AN}}_{\mathrm{max}}$, were computed over 17 Arctic regions (shown in Figure 1): the Bering Sea (BerS), Chukchi Sea (ChuS), Beaufort Sea (BeaS), Hudson Strait (HudS), Davis Strait (DavS), Baffin Bay (BafB), East Siberian Sea (EasS), North Atlantic Ocean (NorA), Hudson Bay (HudB), The Northwestern Passages (TheN), Arctic Ocean West (ArOW), Arctic Ocean E (ArOE), Barents Sea (BarS), Greenland Sea (GreS), Kara Sea (KarS), Laptev Sea (LapS), and the Norwegian Sea (NorS). These 17 regions follow the definitions of the World Seas International Hydrographic

Organization v2, (https://www.marineregions.org, accessed October 2018), with the exception of the Arctic Ocean, which was further divided into two areas for homogeneity purposes, and to capture the changes more influenced by the Atlantic Ocean, as opposed to the changes in the western Arctic. We also calculated the corresponding climatological values for the historical and future periods and the trend for the whole period 1979–2100 (by concatenating the historical and future time series and allowing for a gap of data for the period of 2006–2080). Relative trends were calculated as a percentage of the 1986–2005 reference climate (IPCC, 2013). These quantities were derived for each wave ensemble member and then averaged over the whole ensemble using the democracy approach (Knutti, 2010). The Student t test (von Storch & Zwiers, 2001) at 5% significance level was conducted to determine whether or not the ensemble average of projected changes, or projected trends, is statistically significantly different from zero. For representativeness purposes, the trend analysis of the monthly time series was only performed if at least 10 (positive) data points were available for the historical period and if the corresponding wave area accounted for at least 5% of the total area of analysis.

A preliminary analysis revealed a negligible correlation between $\{H_s\}_{\max}^{\mathrm{MON}}$ and the monthly mean (or maxima) of wave area whereas a correlation above 0.7 is generally found between $\{H_s\}_{\max}^{\mathrm{MON}}$ and the corresponding value for the wind speed in the wave areas (with the exception of the areas more exposed to swells) (see Figure S1 in the supporting information). As in Waseda et al. (2018), this indicates that strong winds need to occur for large waves to develop and that the existence of ice-free areas alone is not enough to explain the occurrence of large waves. We therefore focused on the wind speed in the wave areas, denoted as $\mathrm{U10}^{w}$, taking it as the main predictor for the changes in $\{H_s\}_{\max}^{\mathrm{MON}}$. We compared the aforementioned annual/monthly H_s statistics with those derived from $\mathrm{U10}^{w}$. Specifically, we used the annual/monthly regional maximum of the square value of the wind, denoted as $\{\mathrm{U10}^{w2}\}_{\max}^{\mathrm{MON}}$ and $\{\mathrm{U10}^{w2}\}_{\max}^{\mathrm{AN}}$ because of the quadratic relationship between H_s and wind speed for fully developed wind sea states (Holthuijsen, 2007). To explore the role of the available extension of wave areas in limiting wave growth, we define

$$\mathrm{U10}_{\mathrm{fetch}}^{w2} = \mathrm{U10}^{w2} \times A_{\mathrm{fetch}} \tag{1}$$

with

$$A_{\mathrm{fetch}} = [\tanh(k(gF/\mathrm{U10}^{w2})^{m})]^{p}, \tag{2}$$

where $k = 4.41 \times 10^{-4}$, $m = 0.79$, $p = 0.572$, $g = 9.81\ \mathrm{m/s^2}$, and F is the fetch (Holthuijsen, 2007). A_{fetch} ranges from 0 to 1. $\mathrm{U10}_{\mathrm{fetch}}^{w2}$ accounts for fetch-limited conditions based on the growth curves of H_s in deep water (Holthuijsen, 2007). $\mathrm{U10}_{\mathrm{fetch}}^{w2}$ is therefore based on the assumption of a quadratic relationship for fully developed sea for fetch limited domains, which we think it is a reasonable assumption, because according to the growth curves, fetch-limited wave height is the product of the nonlimited wave height and the fetch factor (equation (2)), while the nonlimited wave height is considered to be proportional to the squared surface wind speed, following the same logic as for the wind predictor that does not consider fetch limitation ($U10^{w2}$). Changes in duration limitation were not accounted for, but they likely play a secondary role compared to changes in fetch.

For each grid point and time step, we approximated the fetch F as the minimum of the following two distances along the local wind direction: (i) the distance to the nearest coastline and (ii) the distance to the nearest grid point with SIC > 75%. Note that this is a simplified approximation of fetch, in which partially ice-covered areas were included in the calculation of the fetch F. To reduce the computational cost, the fetch computation was performed with a daily resolution using the daily SIC maps, the daily average of the $\mathrm{U10}^{w}$ direction, and the daily maximum of $U10^{w}$ magnitude. This is reasonable due to the daily resolution of SIC, which is the variable that mostly contributes to $\mathrm{U10}_{\mathrm{fetch}}^{w2}$ changes by means of modifying the available fetch. The use of the daily maximum wind speed aims to better capture extremal wave heights and considers that cyclones in the Arctic typically last a few days (Sepp & Jaagus, 2011). Wave growth could presumably be limited by duration; however, projected changes of such duration-limited conditions are expected to be small in comparison to the notable changes in fetch. Therefore, the limitation by duration is omitted here, and we focus on future changes rather than historical/future estimates. We use the daily mean wind direction to have a more robust estimate as small variations in direction can cause large variations in fetch. Subsequently, the annual/monthly regional maximum of $\mathrm{U10}_{\mathrm{fetch}}^{w2}$, denoted as $\{\mathrm{U10}_{\mathrm{fetch}}^{w2}\}_{\max}^{\mathrm{MON}}$ and $\{\mathrm{U10}_{\mathrm{fetch}}^{w2}\}_{\max}^{\mathrm{AN}}$, was computed for the trend analysis described above.

The increased extension of wave bodies affects the regional wave maxima not only by reducing the fetch limitation on wave growth; it also affects the probability of strong winds to occur over wave areas (as opposed to occur over densely ice-covered areas), thereby affecting the wind energy available for wave generation and growth. Therefore, the projected changes in $\{U10^{w}\}_{\max}^{MON}$ might be indirectly affected by the increase of the wave areas, in addition to possible changes in winds. In this regard, the following questions arise: (i) Is $\{U10^{w}\}_{\max}^{MON}$ projected to increase more than $\{U10\}_{\max}^{MON}$ (statistic computed from winds over entire area of analysis)? If so, (ii) can this additional increase be explained by the projected future increase in the spatial and temporal extension of the wave areas? In this study, the first question was addressed by directly computing the ratio F_{N_1}, which compares the projected relative future increases in the $\{U10^{w}\}_{\max}^{MON}$ and $\{U10\}_{\max}^{MON}$ climatologies:

$$F_{N_1} = \frac{\overline{\{U10_{\max}^{w,MON}\}^{fut}}}{\overline{\{U10_{\max}^{w,MON}\}^{hist}}} \frac{\overline{\{U10_{\max}^{MON}\}^{hist}}}{\overline{\{U10_{\max}^{MON}\}^{fut}}}, \tag{3}$$

where overlines denote the average of the monthly time series over the historical (*hist*) and future (*fut*) time periods, as indicated.

The second question was addressed by comparing F_{N_1} with F_{N_2}—the relative increase of the expected maximum value over a certain period/region that can be explained by the maximum probability theory:

$$F_{N_2} = \frac{\overline{(1+\frac{0.29}{\ln(\{N^{MON}\}^{fut})})\sqrt{2\ln(\{N^{MON}\}^{fut})}}}{\overline{(1+\frac{0.29}{\ln(\{N^{MON}\}^{hist})})\sqrt{2\ln(\{N^{MON}\}^{hist})}}}. \tag{4}$$

F_{N_2} assumes that the wind speed at each location and time step is independent and identically distributed with a Rayleigh distribution over each studied area and month. This is a reasonable approach as the distribution of U10 can be approximated by a Weibull distribution with shape parameter relatively close to 2 (Figures S2–S7). Note that, for example, a deviation of the shape parameter from 2 to 3 (with scale parameter 10 and N^{MON} increasing from 10,000 to 20,000) only impacts F_{N_2} by <2%. Equation (4) also assumes that the number of independent realizations (N^{MON}) for which the wind variable can possibly achieve its monthly regional maxima is large (Holthuijsen, 2007). N^{MON} is calculated as the number of wave grid points accumulated over each month, which are weighted by the respective cell size relative to the reference surface (~625 km^2). Note that the SMC grid cells slightly vary in size due to converge of meridians at high latitudes (even with the longitudinal merging of cells) and due to coastal refinement (at ~12.5-km resolution) (Casas-Prat & Wang, 2020). We considered one possible realization per day (rather than the subdaily resolution of the wind speed) to minimize the effect of the dependency between consecutive time steps. In order to account for the dependency among neighboring grid points, we also explored the effect of considering a constant subsampling factor to reduce N^{MON} (e.g., diving N^{MON} by 10, as similarly done by Waseda et al. (2018)).

3. Results and Discussion

As shown in Figure 1, the ensemble average of projected changes in climatological mean values of $\{H_s\}_{\max}^{AN}$ is positive and statistically significant for ChuS, BeaS, EasS, HudB, TheN, ArOW, ArOE, GreS, KarS, and LapS. ArOE has the largest ensemble-average projected change, about 3-m increase or up to 80% increase relative to the historical mean. The surrounding KarS, LapS, BeaS, and EasS also show statistically significant increases of above 2 m. The ensemble-average projected changes are negative but statistically insignificant in NorA and NorS.

In terms of the $\{H_s\}_{\max}^{AN}$ trends (not shown), the largest value is also found in ArOE (~3 cm/year), followed by ArOW, BeaS, KarS, LapS, and EasS (1.7–2.7 cm/year). The other statistically significant trends range from 0.5 to 1 cm/year. Unlike the projected changes in the climatological mean value of $\{H_s\}_{\max}^{AN}$ in GreS, its corresponding trend is statistically significant only at the 6% level, not 5%. In the Atlantic side of the domain, $\{H_s\}_{\max}^{AN}$ tends to decrease but insignificantly. Relative to the 1986–2005 climate (Figure 2a), these trends are up to 0.8%/year in ArOE and exceed 0.5%/year in BeaS, EasS, ArOW, KarS, and LapS. However, the latter is not statistically significant due to the larger intra-ensemble variability.

As expected, the relative trends of $\{U10^{w}\}_{\max}^{AN}$ are significantly lower than the corresponding values of $\{H_s\}_{\max}^{AN}$ (Figure 2a vs. Figure 2b) with a maximum of 0.24%/year in ArOE. This does not necessarily entail

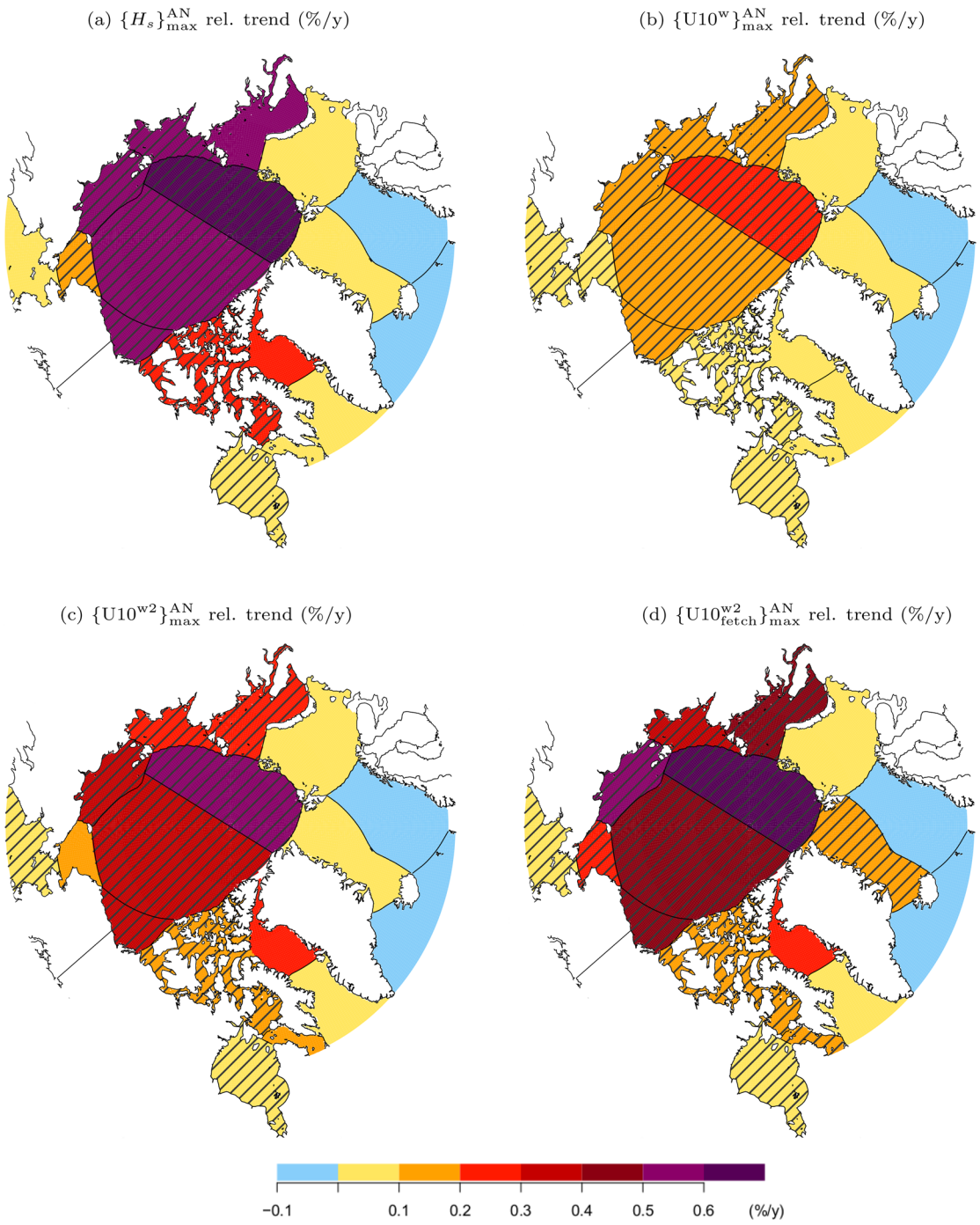

Figure 2. Ensemble average of the trend expressed in percent of the reference period (1986–2005) for (a) $\{H_s\}^{AN}_{max}$, (b) $\{U10^w\}^{AN}_{max}$, (c) $\{U10^{w2}\}^{AN}_{max}$, and (d) $\{U10^{w2}_{fetch}\}^{AN}_{max}$. Hatching indicates statistically significant trends at the 5% significance level.

that wind changes are not a major contributor to H_s changes. In fact, the relative trend of $\{U10^{w2}\}^{AN}_{max}$ (Figure 2c) shows relative increases larger than ~0.5%/year in ArOE (and larger than 0.3%/year in EasS, ArOW and BeaS), which is closer to what is shown for $\{H_s\}^{AN}_{max}$ (Figure 2a). Although a fraction of the $\{H_s\}^{AN}_{max}$ relative trend remains unexplained by wind speed alone, this result suggests that the contribution of the wind speed to long-term H_s changes would be underestimated if the nonlinear nature of the wind-sea states were not taken into account.

The discrepancies between the relative trends of $\{H_s\}^{AN}_{max}$ and wind-derived predictors diminish when incorporating the fetch limitation in $\{U10^{w2}_{fetch}\}^{AN}_{max}$ (Figure 2a vs. Figure 2d). The relative trend of $\{U10^{w2}_{fetch}\}^{AN}_{max}$ is up to 0.9%/year in ArOE, similar to $\{H_s\}^{AN}_{max}$. This indicates the influence of the increasing fetch in projected increases of $H_{s\,max}^{AN}$. It is not surprising that $\{U10^{w2}_{fetch}\}^{AN}_{max}$-derived trends are still generally lower than those of $\{H_s\}^{AN}_{max}$, as the wind predictor does not include the long-term reduction of the local attenuation of waves produced by SIC (for SIC ranging from 25% to 75%) nor the contribution of swell waves. These results are also limited by the inclusion of partially ice-covered areas in the calculation of F, as it deviates from the ice-free assumption in the underlying growth curves theory used in A_{fetch}.

To better understand the regional fetch influence, we looked into the average fetch conditions associated to $\{U10^{w2}_{fetch}\}^{AN}_{max}$ for the historical and future periods (Figure 1). Note that these do not result from the maximum available fetches for each period but from the fetch conditions linked to the co-occurrence of energetic winds and larger fetches so that $U10^{w2}_{fetch}$ maximizes (which are the conditions potentially linked to H_s maxima). It is interesting to note that the more(less)-energetic wave regions are generally linked to the larger (lower) fetches. Statistical significant changes are obtained for ArOE, ArOW, ChuS, BeaS, TheN, EasS, LapS, and GreS, which were some of the areas exhibiting more discrepancies between the relative trends of $\{U10^{w2}\}^{AN}_{max}$ and $\{U10^{w2}_{fetch}\}^{AN}_{max}$. This suggests that fetch plays a particularly important role in these areas. In GreS, however, the rate of $\{U10^{w2}_{fetch}\}^{AN}_{max}$ increase is almost double the corresponding value for $\{H_s\}^{AN}_{max}$ (Figure 2a), which could be explained by larger wind-driven waves being partially counteracted by lower propagated waves coming from the Atlantic (where $\{U10^{w}\}^{AN}_{max}$ tends to decrease). Note that the wind predictors analyzed in this study only account for regionally generated waves and therefore they might fail to represent $\{H_s\}^{AN}_{max}$ in areas largely exposed to swells, like the Atlantic side of the studied domain.

The increase in $\{H_s\}^{AN}_{max}$ is accompanied by a delay of the month in which $\{H_s\}^{AN}_{max}$ occurs (Figure S8), consistent with Casas-Prat and Wang (2020). This is more accentuated in ArOE, ArOW, BafB, HudB, TheN, ChuS, BeaS, EasS, LapS, and KarS. In the future projections $\{H_s\}^{AN}_{max}$ occurs more in December and January, in detriment of August and September. In addition, there is a northward shift of the centroid locations associated to $\{H_s\}^{AN}_{max}$ in latitudes north of 70° N (Figure S8). The shift in the seasonality of $\{H_s\}^{AN}_{max}$ (and $\{U10^{w}\}^{AN}_{max}$, not shown) poses the question of whether the increases in $\{H_s\}^{AN}_{max}$ are mainly the result of extending the ice-free season to more energetic wind seasons or whether the regional H_s extreme wave climate is expected to significantly increase in a given season. Figure 3 gives insight in this matter by illustrating the relative trends of $\{H_s\}^{MON}_{max}$, and the associated wind-derived predictors.

$\{H_s\}^{MON}_{max}$ relative trends are positive and statistically significant in the ArOE, ArOW, BeaS, EasS, TheN, and LapS for most of the summer months (Figure 3a). Larger values usually occur in the transitional months, that is, at the beginning and/or end of the ice-free season when changes in SIC are larger (Figure S9). Statistically significant trends are of the same order of magnitude as corresponding values for $\{H_s\}^{AN}_{max}$. This suggests that the $\{H_s\}^{AN}_{max}$ projected increases are affected not only by changes in time of $\{H_s\}^{AN}_{max}$ occurrence but also by an actual increase in $\{H_s\}^{MON}_{max}$. The relative trends of $\{U10^{w2}\}^{MON}_{max}$ (Figure 3b) are generally lower and less statistically significant. After including the fetch factor with $\{U10^{w2}_{fetch}\}^{MON}_{max}$, relative trends become closer to those of $\{H_s\}^{MON}_{max}$, which illustrate the fetch influence at monthly scale (Figure 3a vs. Figure 3c).

We found that the influence of the sea ice retreat on the monthly regional maximum waves is not limited to the fetch-limited wave growth. Sea ice retreat also favors the increase of $\{U10^{w2}\}^{MON}_{max}$. This is revealed by comparing the relative trends of $\{U10^{w2}\}^{MON}_{max}$ and $\{U10^{2}\}^{MON}_{max}$ (Figure 3b vs. Figure 3d). Results for $\{U10^{2}\}^{MON}_{max}$ do not capture the increases found for $\{U10^{w2}\}^{MON}_{max}$ for some months in the Arctic Ocean and surrounding seas. $\{U10^{2}\}^{MON}_{max}$ trends are in agreement with the projected changes in the monthly maximum U10 at each grid point, which barely exhibit statistically significant changes (Figure S10). The fact that the differences between $\{U10^{w2}\}^{MON}_{max}$ and $\{U10^{2}\}^{MON}_{max}$ trends are larger during the transitional months, when larger changes between the historical and future ice-covered areas are expected, suggests that the increase in $\{U10^{w2}\}^{MON}_{max}$ might be largely influenced by the spatial and temporal extension of the sea ice area. Indeed, F_{N_1} (equation (4)) is mostly >1 for these months, indicating larger projected changes in $\{U10^{w}\}^{MON}_{max}$ in comparison to $\{U10\}^{MON}_{max}$ (Figure S12a).

F_{N_2} overestimates F_{N_1} but gives a similar monthly/spatial pattern with similar order of magnitudes (Figure S12b). The discrepancies between F_{N_1} and F_{N_2} exacerbate when including a resampling factor in N^{MON} to account for spatial dependency. The reasons behind these discrepancies are probably due to the

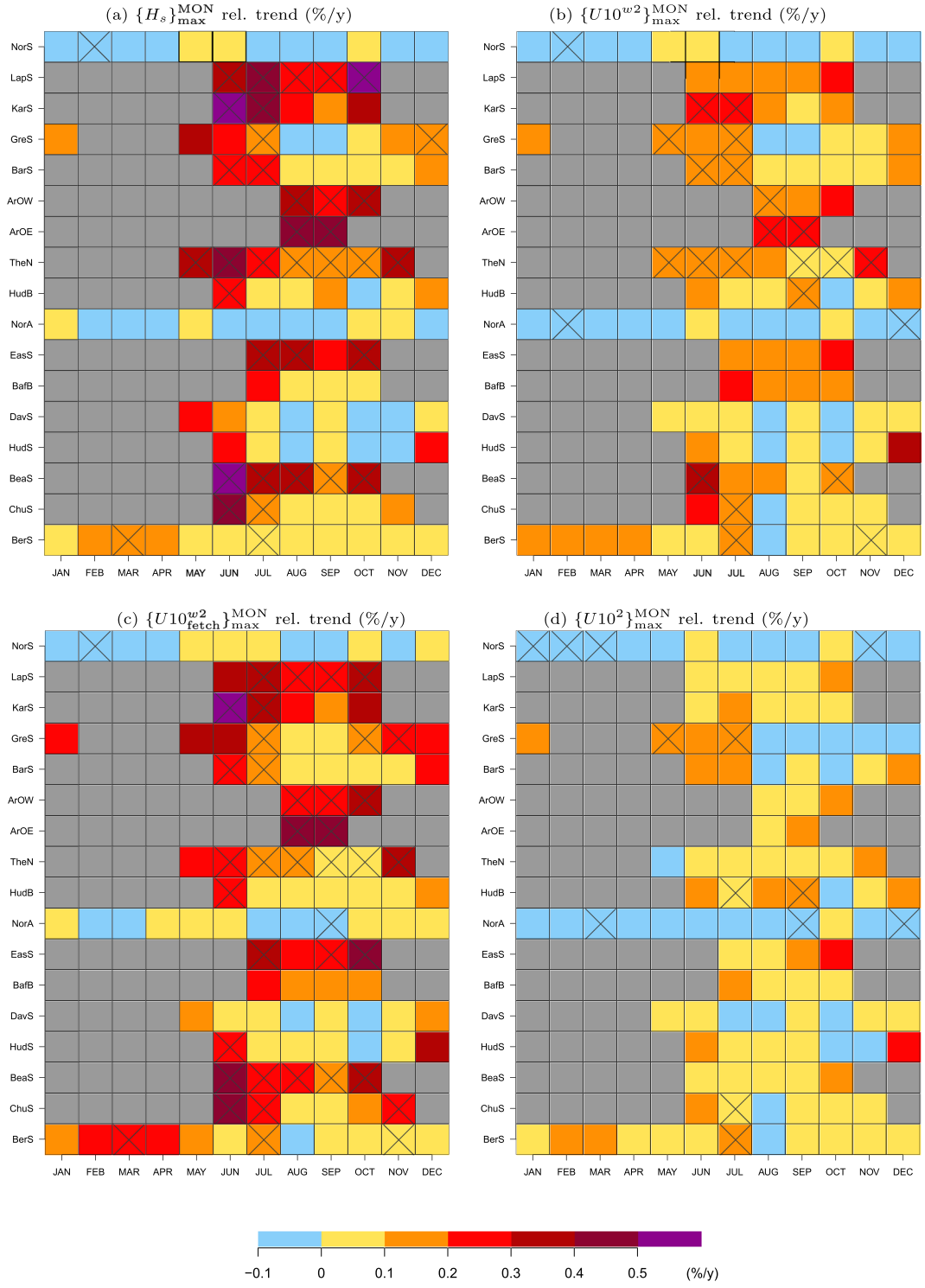

Figure 3. Ensemble average of the trend relative to the period 1986–2005 for the following variables: (a) $\{H_s\}^{\mathrm{MON}}_{\mathrm{max}}$, (b) $\{U10^{w2}\}^{\mathrm{MON}}_{\mathrm{max}}$, $\{U10^{w2}_{\mathrm{fetch}}\}^{\mathrm{MON}}_{\mathrm{max}}$, and $\{U10\}^{2MON}_{\mathrm{max}}$. Trends were not computed in the gray months due to minimal ice-free conditions for the historical period. Crosses indicate statistically significant trends at the 5% significance level.

assumptions inherent to the maximum probability theory used to calculate F_{N_2}. Despite U10 being reasonably fitted by a Weibull distribution (with shape parameter close to 2) (Figures S2–S7), U10 is likely not perfectly homogeneous over the studied areas, in particular in larger or orography-complex areas. In addition, the increased heat flux from the ocean to the atmosphere and associated turbulence over open water areas can induce changes in winds (Vihma et al., 2014; Vichi et al., 2019), meaning that the probability of large winds to achieve its maximum over a water cell or an ice-covered cell could be different. Therefore, F_{N_2} might not be the only factor that explains the intensified changes in $\{U10^{w}\}^{MON}_{max}$, as compared to $\{U10\}^{MON}_{max}$, which ultimately affects $\{H_s\}^{MON}_{max}$. However, the similarity between F_{N_2} and F_{N_2} indicates that the increasing extension of wave areas plays a relevant role toward explaining the increase in effective U10 that drives $\{H_s\}^{MON}_{max}$.

We can therefore qualitatively assess the contribution of sea ice retreat on $\{H_s\}^{MON}_{max}$ (by means of increasing fetch) as the difference between the projected increases in $\{U10^{w2}_{fetch}\}^{MON}_{max}$ and $\{U10^{w2}\}^{MON}_{max}$, respectively. Similarly, the differences between the projected increases in $\{U10^{w2}\}^{MON}_{max}$ and $\{U10^{2}\}^{MON}_{max}$ illustrate the contribution of the sea ice retreat on $\{H_s\}^{MON}_{max}$ (by means of increasing the expected value of the maximum regional winds as a result of widening and lengthening the wave areas). These contributions are relevant in most of the studied regions, but they seem to both be particular notable in BeaS, EasS, ArOE, ArOW, KarS, and LapS (Figures S12–S13).

4. Conclusions

This study analyzed the projected changes and trends of the annual/monthly regional maximum of H_s, $\{H_s\}^{AN}_{max}$ and $\{H_s\}^{MON}_{max}$, in the Arctic region (including the Hudson Bay). These projections were derived from five sets of CMIP5-derived wave climate simulations for the historical (1979–2005) and the future (2081–2100) period under the RCP8.5 emission scenario, which were presented in Casas-Prat and Wang (2020).

The results show that $\{H_s\}^{AN}_{max}$ is projected to increase 2- to 3-m in average in the ArOE, ArOW, BeaS, EasS, LapS, and KarS. Lower but statistically significant positive changes were also found in ChuS, HudB, TheN, and GreeS. These projected changes entailed trends up to 3 cm/year (exceeding 0.5%/year relative to the reference 1986–2005 climate in many regions surrounding the Arctic Ocean). The area exhibiting the largest relative trends is the ArOE, with up to 0.8%/year. In addition, the locations associated with $\{H_s\}^{AN}_{max}$ tend to shift northward in latitudes north of 70° N.

Our results also showed that if the nonlinear relationship between H_s and wind speed for wind-sea states was not taken into account, the contribution of wind to increasing H_s can be underestimated. Although strong winds need to occur for large waves to occur, we found that the wind speed alone cannot explain the projected increases in $\{H_s\}^{AN}_{max}$. With the attempt to reduce this gap, we build a wind predictor that accounted for the influence of sea ice retreat by including the fetch-limiting factor. Such predictor was found to explain a large fraction of the relative trends of $\{H_s\}^{AN}_{max}$. The areas where the fetch increase was found to be more relevant are the ArOE, ArOW, BeaS, EasS, LapS, and GreS. In the latter, however, the swell influence seems to partially counteract the sea ice retreat influence on the regional annual maximal wave heights.

The monthly regional analysis confirmed the influence of fetch on the increases in $\{H_s\}^{MON}_{max}$. It also revealed that the relative trends associated to the wind speed over wave areas seem to be largely affected by the increased temporal and spatial extension of the water areas. That is not to say that projected increases in the regional maxima of wind speed (whether over ice or water) will not occur but the ensemble average obtained in this study barely exhibits statistically significant increases.

Therefore, we conclude that sea ice retreat notably contributes to increasing the regional maxima of H_s by reducing fetch limitation and also by increasing the chance for strong winds to occur in water areas. Another effect that is relevant, and was not quantified in this study, is the sea ice-retreat impact on reducing the local wave attenuation caused by SIC. Further work based on a larger ensemble of wave projections is needed to derive more robust results. A larger ensemble should involve not only more combinations of U10/SIC forcing fields (resulting from different models and scenarios) but also different wave modeling methodologies with different SIC approaches to better reproduce the complex wave-ice interaction mechanisms, as more information about the future sea ice states becomes available. Moreover, to better understand trends of wave

heights over a changing domain in time and space, more complex statistical analysis might be adopted in future studies to gain insight into the underlying regional changes.

Data Availability Statement

Data can be accessed at the Government of Canada's Open Data Portal under Arctic regional maximum wave heights and trends derived from CMIP5based ocean wave simulations for the periods 19792005 and 20812100 (https://open.canada.ca/data/en/dataset/2c1717e8-c742-4ecd-8266-0a823851fdd2).

Acknowledgments
The authors acknowledge the World Climate Research Programme's Working Group on Coupled Modelling, which is responsible for CMIP, and we thank the climate modeling groups (BCC-CSM1-1, INMCM4, MIROC5, GFDL-ESM2M, and EC-EARTH) for producing and making available their model output. For CMIP the U.S. Department of Energy's Program for Climate Model Diagnosis and Intercomparison provides coordinating support and led development of software infrastructure in partnership with the Global Organization for Earth System Science Portals. The authors are also grateful to Joao Morim for his comments on an earlier version of this manuscript.

References

AMSA (2009). Arctic Marine Shipping Assessment 2009 report. Arctic Council.

Aksenov, Y., Popova, E. E., Yool, A., Nurser, A. J. G., Williams, T. D., Berino, L., & Bergh, J. (2017). On the future navigability of Arctic sea routes: High-resolution projections of the Arctic Ocean and sea ice. *Marine Policy*, *75*, 300–317. https://doi.org/10.1016/j.marpol.2015.12.027

Alberello, A., Onorato, M., Bennetts, L., Vichi, M., Eayrs, C., MacHutchon, K., & Toffoli, A. (2019). Brief communication: Pancakge ice flow size distribution during the winter expansion of the Antarctic marginal ice zone. *The Cryosphere*, *13*, 41–48. https://doi.org/10.5194/tc-13-41-2019

Ardhuin, F., Rogers, E., Babanin, A., Filipot, J. F., Magne, R., Roland, A., & Collard, F. (2010). Semiempirical dissipation source functions for ocean waves. Part I: Definition, calibration, and validation. *Journal of Physical Oceanography*, *40*, 1917–1941. https://doi.org/10.1175/2010JPO4324.1

Boutin, G., Lique, C., Ardhuin, F., Rousset, C., Talandier, C., Accensi, M., & Girard-Ardhuin, F. (2020). Towards a coupled model to investigate wave-sea ice interactions in the Arctic marginal ice zone. *The Cryosphere*, *14*, 709–735. https://doi.org/10.5194/tc-14-709-2020

Casas-Prat, M., & Wang, X. L. (2020). Projections of extreme ocean waves in the Arctic and potential implications for coastal inundation and erosion. *Journal of Geophysical Research: Oceans*, *125*, e2019JC015745. https://doi.org/10.1029/2019JC015745

Copernicus Climate Change Service (C3S) (2017). ERA5: Fifth generation of ECMWF atmospheric reanalyses of the global climate.

Doble, M., & Bidlot, J. R. (2013). Wave buoy measurements at the Antarctic sea ice edge compared with an enhanced ECMWF WAM: Progress towards global waves-in-ice modelling. *Ocean Modelling*, *70*, 166–173. https://doi.org/10.1016/j.ocemod.2013.05.012

Hasselmann, S., & Hasselman, K. (1985). Computations and parameterizations of the nonlinear energy transfer in a gravity-wave spectrum, Part I: A new method for efficient computations of the exact nonlinear transfer integral. *Journal of Physical Oceanography*, *15*, 1369–1377.

Hemer, M. A., Wang, X. L., Charles, E., Hegermiller, C., & COWCLIP contributors (2014). Report of the 2014 Meeting for the WCRP-JCOMM Coordinated Global Wave Climate Projections (COWCLIP). JCOMM Oceanography and Marine Meteorology.

Holthuijsen, L. (2007). *Waves in oceanic and coastal waters*. Cambridge: Cambridge University Press.

IPCC (2013). Climate Change 2013: The Physical Science Basis. Contribution of Working Group I to the Fifth Assessment Report of the Intergovernmental Panel on Climate Change. In T. F. Stocker et al. (Eds.) (1535 pp.). Cambridge, United Kingdom and New York, NY, USA: Cambridge University Press. https://doi.org/10.1017/CBO9781107415324

Khon, V. C., Mokhov, I. I., Pogarskiy, F. A., Dethloff, K. A., Rinke, A., & Matthes, H. (2014). Wave heights in the 21st century Arctic Ocean. *Geophysical Research Letters*, *41*, 2956–2961. https://doi.org/10.1002/2014GL059847

Knutti, R. (2010). The end of model democracy? *Climatic Change*, *102*, 395–404. https://doi.org/10.1007/s10584-010-9800-2

Kohout, A. L., & Meylan, M. H. (2008). An elastic plate model for wave attenuation and ice floe breaking in the marginal ice zone. *Journal of Geophysical Research*, *113*, C09016. https://doi.org/10.1029/2007JC004434

Kohout, A., Williams, M. J., Dean, S. M., & Meylan, M. (2014). Storm-induced sea-ice breakup and the implications for ice extent. *Nature*, *509*(7502), 604–7. https://doi.org/10.1038/nature13262

Laliberté, F., Howell, S., & Kushner, P. (2016). Regional variability of a projected sea ice-free Arctic during the summer months. *Geophysical Research Letters*, *43*, 256–263. https://doi.org/10.1002/2015GL066855

Li, J. G. (2012). Propagation of ocean surface waves on a spherical multiple-cell grid. *Journal of Computational Physics*, *231*(24), 8262–8277. https://doi.org/10.1016/j.jcp.2012.08.007

Li, J. G. (2016). Ocean surface waves in an ice free Arctic ocean. *Ocean Dynamics*, *66*, 989–1004. https://doi.org/10.1007/s10236-016-0964-9

Liu, Q., Babanin, A. V., Zieger, S., Young, I. R., & Guan, C. (2016). Wind and wave climate in the Arctic Ocean as observed by altimeters. *Journal of Climate*, *29*, 7957–7975. https://doi.org/10.1175/JCLI-D-16-0219.1

Liu, Q., Rogers, W. E., Babanin, A., Li, J., & Guan, C. (2020). Spectral modelling of ice-induced wave decay. *Journal of Physical Oceanography*, *50*(6), 1583–1604. https://doi.org/10.1175/JPO-D-19-0187.1

Meylan, M. H., Bennetts, L. G., & Kohout, A. L. (2014). In situ measurements and analysis of ocean waves in the Antarctic marginal ice zone. *Geophysical Research Letters*, *41*, 5046–5051. https://doi.org/10.1002/2014GL060809

Mioduszewski, J., Vavrus, S., & Wang, M. (2018). Diminishing Arctic sea ice promotes stronger surface winds. *Journal of Climate*, *31*, 8101–8119. https://doi.org/10.1175/JCLI-D-18-0109.1

Morim, J., Hemer, M. A., Wang, X. L., Cartwright, N., Trenham, C., Semedo, A., & Stopa, J. (2019). Robustness and uncertainties in global multivariate wind-wave climate projections. *Nature Climate Change*, *7*, 711–718. https://doi.org/10.1038/s41558-019-0542-5

Rinke, A., Maturilli, M., Graham, R. M., Matthes, H., Handorf, D., Cohen, I., & Moore, J. C. (2017). Extreme cyclone events in the Arctic: Wintertime variability and trends. *Environmental Research Letters*, *12*, 094,006. https://doi.org/10.1088/1748-9326/aa7def

Rogers, W. E., Thomson, J., Shen, H. H., Doble, M. J., Wadhams, P., & Cheng, S. (2016). Dissipation of wind waves by pancake and frazil ice in the autumn Beaufort Sea. *Journal of Geophysical Research: Oceans*, *121*, 7991–8007. https://doi.org/10.1002/2016JC012251

Saha, S., Moorthi, S., Pan, H., Wu, X., Wang, J., Nadiga, S., & Goldberg, M. (2010). The NCEP Climate Forecast System Reananlysis. *Bulletin of the American Meteorological Society*, *91*(8), 1015–1057. https://doi.org/10.1175/2010BAMS3001.1

Semedo, A., Vettor, R., Breivik, Ø., Sterl, A., Reistad, M., Guedes Soares, C., & Lima, D. C. A. (2015). The wind sea and swell waves climate in the Nordic seas. *Ocean Dynamics*, *65*(2), 223–240. https://doi.org/10.1007/s10236-014-0788-4

Sepp, M., & Jaagus, J. (2011). Changes in the activity and tracks of Arctic cyclones. *Climatic Change*, *105*, 577–595. https://doi.org/10.1007/s10584-010-9893-7

Shu, Q., Song, Z., & Qiao, F. (2015). Assessment of sea ice simulations in the CMIP5 models. *The Cryosphere*, *9*, 399–409. https://doi.org/10.5194/tc-9-399-2015

Squire, V. A. (2020). Ocean wave interactions with sea ice: A reappraisal. *Annual Review of Fluid Mechanics*, *52*, 37–60. https://doi.org/10.1146/annurev-fluid-010719-060301

Stopa, J., Ardhuin, F., & Girard-Ardhuin, F. (2016). Wave climate in the Arctic 1992–2014: Seasonality and trends. *The Cryosphere*, *10*, 1605–1629. https://doi.org/10.5194/tc-10-1605-2016

Taylor, K. E., Stouffer, R. J., & Meehl, G. A. (2012). An overview of CMIP5 and the experiment design. *Bulletin of the American Meteorological Society (BAMS)*, *93*(4), 485–498. https://doi.org/10.1175/BAMS-D-11-00094.1

The WAVEWATCH III Development Group (WW3DG) (2016). User manual and system documentation of WAVEWATCH III Version 5.16. NOAA/NWS/NCEP/MMAB, College Park, MD, USA.

Thomson, J., Ackley, S., Girard-Ardhuin, F., Ardhuin, F., Babanin, A., Boutin, G., & Wadhams, P. (2018). Overview of the Arctic Sea state and boundary layer physics program. *Journal of Geophysical Research: Oceans*, *123*, 8674–8687. https://doi.org/10.1002/2018JC013766

Thomson, J., Fan, Y., Stammerjohn, S., Stopa, J., Rogers, E., Girard-Ardhuin, F., & Bidlot, J. R. (2016). Emerging trends in the sea state of the Beaufort and Chukchi seas. *Ocean Modelling*, *105*, 1–12. https://doi.org/10.1016/j.ocemod.2016.02.009

Thomson, J., & Rogers, W. E. (2014). Swell and sea in the emerging Arctic Ocean. *Geophysical Research Letters*, *41*, 3136–3140. https://doi.org/10.1002/2014GLO59983

Tolman, H. (2003). Treatment of unresolved islands and ice in wind wave models. *Ocean Modelling*, *5*(3), 219–231. https://doi.org/10.1016/S1463-5003(02)00040-9

Vichi, M., Eayrs, C., Alberello, A., Bekker, A., Bennetts, L., Holland, D., et al. (2019). Effects of an explosive polar cyclone crossing the Antarctic Marginal Ice zone. *Geophysical Research Letters*, *46*, 5948–5958. https://doi.org/10.1029/2019GL082457

Vihma, T., Pirazzini, R., Fer, I., Renfrew, I., Sedlar, J., Tjernström, M., & Gascard, J. (2014). Advances in understanding and parametrization of small-scale physical processes in the marine Arctic climate system: A review. *Atmospheric, Chemistry and Physics*, *14*, 9403–9450. https://doi.org/10.5194/acp-14-9403-2014

von Storch, H., & Zwiers, W. (2001). *Statistical analysis in climate research*. Cambridge, UK: Publisher Cambridge.

Wang, X. L., Feng, Y., Swail, V., & Cox, A. (2015). Historical changes in the Beaufort-Chukchi-Bering seas surface winds and waves, 1971–2013. *Journal of Climate*, *28*, 7457–7458. https://doi.org/10.1002/2014JC010087

Wang, X., Hemer, M., & COWCLIP contributors (2015). Report of the 2015 Meeting for the WCRP-JCOMM Coordinated Global Wave Climate Projections (COWCLIP). JCOMM Oceanography and Marine Meteorology.

Waseda, T., Webb, A., Sato, K., Inoue, J., Kohout, A., Penrose, B., & Penrose, S. (2018). Correlated increase of high ocean waves and winds in the ice-free waters of the Arctic Ocean. *Nature Scientific Reports*, *8*, 4489. https://doi.org/10.1038/s41598-018-22500-9

Zhang, X., Walsh, J., Zhang, J., Bhatt, U. S., & Ikeda, M. (2004). Climatology and interannual variability of Arctic cyclone activity: 1948–2002. *Journal of Climate*, *17*, 2300–2317. https://doi.org/10.1175/1520-0442(2004)017